

## Links between Tropical Cyclone Activity and Madden–Julian Oscillation Phase in the North Atlantic and Northeast Pacific Basins

BRADFORD S. BARRETT

*School of Meteorology, University of Oklahoma, Norman, Oklahoma, and Department of Geophysics, Faculty of Physical Sciences and Mathematics, University of Chile, Santiago, Chile*

LANCE M. LESLIE

*School of Meteorology, University of Oklahoma, Norman, Oklahoma*

(Manuscript received 21 March 2008, in final form 11 August 2008)

### ABSTRACT

The leading intraseasonal mode of atmospheric and oceanic variability, the Madden–Julian oscillation (MJO), influences tropical and extratropical sea level pressure, temperature, divergent and rotational wind components, moisture, and deep convection. As a 40- to 50-day oscillation, the MJO is also known to influence tropical phenomena, including tropical cyclone (TC) activity in various TC basins. The links between the MJO and multiple measures of TC activity, including genesis, landfall, and an integrative accumulated cyclone energy (ACE) index, were quantified for multiple TC-formation basins across the Western Hemisphere, including the North Atlantic and northeast Pacific Ocean and subbasins, for the period 1978–2006. Using this relatively long (29 yr) TC dataset and employing an upper-tropospheric MJO diagnostic that is physically meaningful over the entire Western Hemisphere, this study extends existing research on the relationships between the MJO and TCs. The NOAA Climate Prediction Center’s operational MJO index, derived from 200-hPa velocity potential data, was divided into three phases. Relative frequencies of the MJO phases were compared with observed levels of TC activity using a binomial distribution hypothesis test. The MJO was found to statistically significantly modulate the frequency of TC genesis, intensification, and landfall in the nine TC basins studied. For example, when an MJO index was large and positive at 120°W, hurricanes and intense hurricanes were 4 times as likely to make landfall in the North Atlantic. This modulation of TC activity, including landfall patterns in the North Atlantic, was physically linked to the upper-atmospheric response to the eastward-propagating MJO and is evident as a dipole of TC activity between Pacific and Atlantic subbasins.

### 1. Introduction

Increasing our understanding and predictive capability of tropical cyclogenesis is a fundamental goal of tropical cyclone (TC) research, as such an increase would allow for more rapid planning and responses to possible TC activity. Tropical cyclone research has mostly concentrated on two ends of the time spectrum: short-range forecasting of the track and intensity of an existing TC out to about five days, and predicting seasonal and longer levels of TC activity. Advances in near-real-time forecasts have come primarily through im-

provements in numerical weather prediction (NWP) and in statistical–climatological models (Powell and Abernethy 2001; Franklin et al. 2003; Barrett et al. 2006). Beyond this time scale, in the 5- to 20-day window, initialization errors and chaotic atmospheric variability lead to diminishing atmospheric predictability from dynamical NWP models (e.g., Leslie et al. 1989; Quan et al. 2004). Gray (1979) observed that North Atlantic Ocean tropical cyclogenesis tends to cluster in time, with a two- to three-week period of multiple instances of TCs, followed by a two- to three-week period of few to no occurrences of cyclogenesis. This temporal periodicity suggests a connection to an intraseasonal mode of variability, such as the Madden–Julian oscillation (MJO; Madden and Julian 1971, 1972). It is in this window that accurate guidance, particularly in forecasting cyclogenesis, would prove highly useful (Hall

---

*Corresponding author address:* Bradford Barrett, Department of Geophysics, University of Chile, Blanco Encalada 2002, Santiago, Chile.

E-mail: bbarrett@dgf.uchile.cl

TABLE 1. Definitions, geographic regions, and abbreviations of the nine basins examined for this study.

Basin	Latitude		Longitude		Abbreviation
	South	North	East	West	
Northeast Pacific		All TCs in the best-track dataset			EPAC
North Atlantic		All TCs in the best-track dataset			NATL
Caribbean	10.0°N	22.0°N	60.0°W	90.0°W	CARIB
Gulf of Mexico	18.0°N	31.0°N	82.5°W	98.0°W	GOM
Eastern northeast Pacific		All latitudes	78.5°W	100.0°W	EEPAC
Central northeast Pacific		All latitudes	100.0°W	115.0°W	CEPAC
Western northeast Pacific		All latitudes	115.0°W	140.0°W	WEPAC
Central Pacific		All latitudes	140.0°W	180.0°W	CPAC
Atlantic main development region	10.0°N	20.0°N	17.5°W	90.0°W	AMDR

et al. 2001; Bessafi and Wheeler 2006), especially for subbasins where the life cycle from initial disturbance to landfall is often only a few days, such as in the Gulf of Mexico, Caribbean Sea, and the northeast Pacific Ocean adjacent to Mexico. Additionally, foreknowledge of TC activity in a specific basin or subbasin clearly benefits operational centers by providing increased time to deploy additional observational tools, schedule satellite intensive operational periods and reconnaissance aircraft, and position buoys. These early preparations for landfalling TC impacts lead to dramatic reductions in loss of life and property (Sheets 1990).

The primary objective of this study is to demonstrate modulation by the MJO of TC activity in nine basins and subbasins spanning the Western Hemisphere. The TC basins, summarized in Table 1 and Fig. 1, include the northeast Pacific (EPAC) and North Atlantic (NATL), as well as seven subbasins of each, including the eastern northeast Pacific (EEPAC), central northeast Pacific (CEPAC), western northeast Pacific (WEPAC), central Pacific (CPAC), Caribbean Sea (CARIB), Gulf of Mexico (GOM), and Atlantic main development region (AMDR; Goldenberg and Shapiro 1996). Using a definition of TC activity, which is categorized by genesis, intensification, and landfall, we quantify the MJO's modulation by contrasting observed TC activity in each basin with expected TC activity during each MJO phase for the period 1978–2006 (section 2 contains a more detailed description of the TC dataset). In this study, TC activity is defined by counts of genesis and landfall of tropical storms (TS), hurricanes (H), and intense hurricanes (IH), as well as by the integrative accumulated cyclone energy (ACE; Bell et al. 2000) index. A TS is defined as a TC with sustained 1-min winds of at least 35 kt (1 kt  $\approx$  0.5 m s<sup>-1</sup>); an H (IH) is defined as a TC with sustained 1-min winds of at least 64 (96) kt (McBride 1981). ACE is computed over the period 1970–2006 as the sum of the squares of the wind speeds for each data point over the lifetime of the TC.

Much complexity, associated with interactions on a variety of temporal and spatial scales, limits the accurate and consistent prediction of TC genesis. The annual mean number of TCs is globally about 90, with a standard deviation of 10. Although these numbers are disputed (Frank and Young 2007), to date no evidence exists of a long-term trend in either the TC global frequency or variability (Kossin et al. 2007; Webster et al. 2005; Emanuel 2005). There is evidence, however, of regional control of TC activity. For example, variability in tropical SSTs and deep tropospheric wind shear are correlated with interannual trends in North Atlantic TC genesis, intensity, and duration (Emanuel 2006; Frank and Young 2007). The TCs are fundamentally connected to both the atmospheric and oceanic general circulation (e.g., Chan 2005; Wu et al. 2007; Ramsay et al. 2008), and thus it is reasonable to expect the dominant modes of tropical and extratropical atmospheric and oceanic variability to have detectable effects on TC activity. However, TC predictability diminishes on time scales beyond about a few days (Bell and Chelliah 2006). Therefore, there is great interest in developing knowledge of the climate factors which control intraseasonal fluctuations in TC activity.

The MJO, discussed in detail by Madden and Julian (1994), originates as synoptic-scale circulation cells oriented in the equatorial plane that propagate eastward from the Indian Ocean into the central Pacific Ocean. A primary phenotypical expression of the oscillation is the enhancement (or suppression) of convective regions, which are observed to propagate eastward (Nakazawa 1986, 1988). Although complete circulation cells do not extend much beyond the eastern hemisphere, zonal wind anomalies in the upper troposphere are observed to circumnavigate the globe (Madden and Julian 1994; Kiladis et al. 2005). Therefore, we will use the term “MJO” to describe the oscillation in all ocean basins, including the North Atlantic and northeast Pacific.

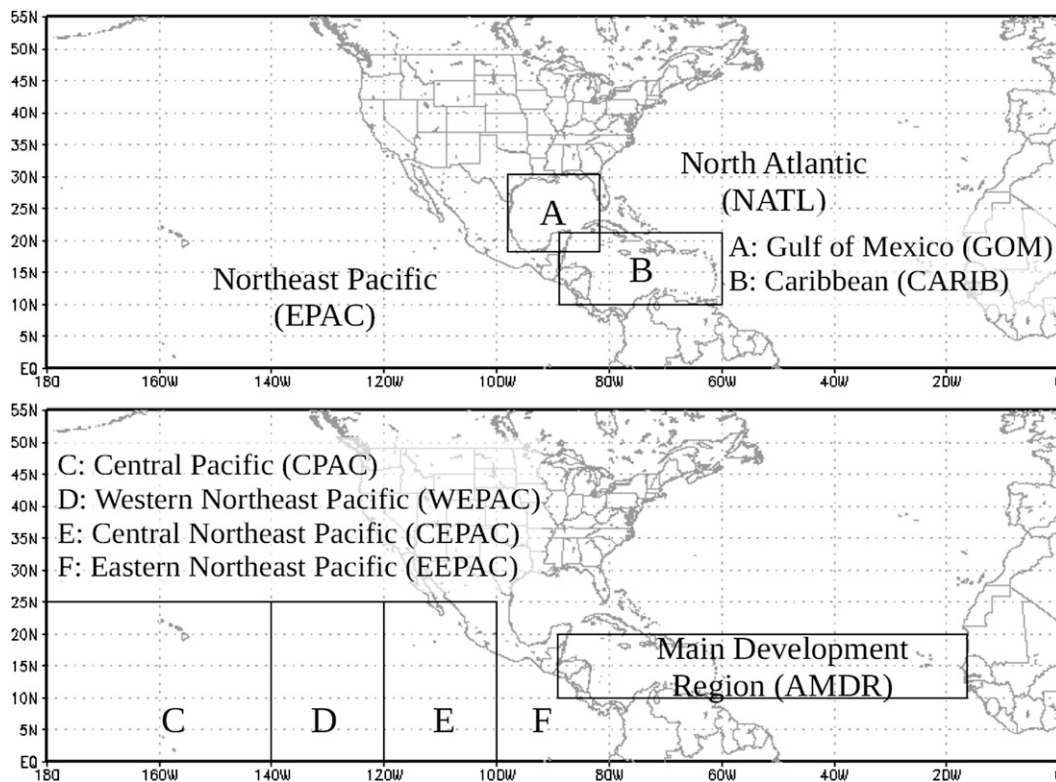


FIG. 1. Locations and acronyms for the nine TC basins examined in this study.

*Previous MJO–TC studies*

There have been many studies since 1986 that examined connections between TC activity and the MJO. However, most have used datasets limited in space or time, or focused on only one basin. Here we attempt to synthesize the previous body of research to date, highlighting the differing methodologies used to determine MJO–TC relationships. Nakazawa (1986) used TC data from the 1979 season to find a modulation of regional TC activity on the 30- to 60-day time scale of the MJO. Von Storch and Smallegange (1991), while limited to a 5-yr period, found connections between outgoing long-wave radiation (OLR) and TCs in the North and South Pacific Oceans. Liebmann et al. (1994) noticed changes in west Pacific TC activity and attributed them to the phase of the MJO and its impact on the meso- and synoptic-scale organization of deep convection. Molinari et al. (1997), examining the 13 TCs that formed in 1991, found a correlation between east Pacific TC genesis and the strength of a potential vorticity gradient in the Caribbean Sea. They attributed this relationship to the enhancement of westward-propagating tropical waves by the MJO. Molinari and Vollaro (2000) further

examined the spatial and temporal patterns of east Pacific TC genesis for the 1991 season, and found that TCs tend to form progressively eastward with time, a result consistent with the eastward propagation of the MJO. Maloney and Hartmann (2000a,b) found strong connections between 850-hPa wind anomalies in the eastern Pacific Ocean and North Pacific, Gulf of Mexico, and Caribbean hurricane activity over 1949–97, with TSs (Hs) 2 (4) times as likely to generate during periods of westerly 850-hPa wind anomalies than during easterly wind anomalies. They attributed the wind anomalies, and their associated production of low-level cyclonic vorticity and horizontal wind shear, to the passage of the eastward-propagating MJO. Mo (2000), using a limited dataset (five selected years from 1976 to 1986), examined OLR anomalies and North Atlantic tropical storm activity and found a teleconnection relationship between positive OLR anomalies (i.e., suppressed convection) in the Indian Ocean and enhanced tropical storm activity in the North Atlantic. Collins and Mason (2000) split the northeast Pacific basin into regional pieces and found TC cyclogenesis over the period 1972–1997 was significantly related to sea surface

temperature, relative humidity, precipitable water content, and vertical velocity. Higgins and Shi (2001) connected 200-hPa velocity potential with TC activity and found a relationship between enhanced convection on the MJO time scale and TC genesis in both the northeast Pacific and North Atlantic from 1979–1997. Hall et al. (2001) quantified the statistical significance of the relationship between the MJO and TC activity for the Australian region for the 20-yr period 1976–1996, and similar to Maloney and Hartmann (2000a,b), attributed the relationship to the MJO's modulation of low-level relative vorticity. Bessafi and Wheeler (2006) documented the modulation for the south Indian Ocean and attributed the modulation to MJO-induced perturbations in low-level relative vorticity and vertical wind shear. Frank and Roundy (2006) found that a composite genesis profile during favorable MJO conditions had an anomalous (easterly) reduction in vertical shear and increased low-level vorticity. Kim et al. (2008) examined the western North Pacific for the period 1979–2004 and found that TC activity increased when the MJO favored deep convection over the basin, and that the density of TC tracks was shifted by the prevailing large-scale steering flow for each MJO phase. Finally, Leroy and Wheeler (2008) developed an intraseasonal statistical prediction scheme for the Southern Hemisphere using the phase of the eastward-propagating MJO (represented by the index of Wheeler and Hendon 2004) as two of five predictors.

This present study extends the current understanding of the relationships between the MJO and TC activity in three main ways: 1) it identifies the MJO from 200-hPa velocity potential anomalies (section 3), a metric that proves globally useful because upper-tropospheric velocity potential anomalies are one of the few phenotypical signals observed to circumnavigate the tropics (e.g., Madden and Julian 1994; Harr and Elsberry 1995; Arguez et al. 2005; Zhang 2005); 2) it uses use 29 yr of best-track data from the geostationary satellite era, providing greater degrees of freedom in deriving statistical significance from our hypothesis tests (most prior studies used 5–20 yr of satellite-era datasets); 3) it suggests that there are multiscale environmental responses to the dry Kelvin wave component of the MJO acting as physical links between the MJO and TC activity, over nine TC basins.

The remainder of this article is organized as follows. Section 2 describes the TC datasets used for the analysis. Section 3 summarizes the methodology; section 4 highlights the results of the research. Section 5 discusses the results and suggests physical mechanisms for the modulation; and section 6 summarizes the study and suggests areas for future work.

## 2. Best-track data

All measures of TC activity used in this study are based on data contained in the North Atlantic and northeast Pacific so-called best-track datasets (Jarvinen et al. 1984). The limitations and inhomogeneities of the best-track datasets have been well documented (e.g., Buckley et al. 2003; Webster et al. 2005; Emanuel 2005; Mann and Emanuel 2006; Klotzbach 2007; Landsea 2007; Frank and Young 2007; Emanuel et al. 2008). However, no other similarly comprehensive data are available and therefore this dataset will be used to compute TC activity in this study. As defined earlier, TC activity is measured using three metrics: cyclogenesis, intensification, and landfall. To determine TC activity from the first two metrics, every point of tropical cyclogenesis was identified for nine different basins and subbasins. The period 1978–2006 was selected to match the period of record of the MJO index (described in section 3).

Tropical cyclogenesis is defined as the first record in the best-track dataset where the TC has at least 35-kt sustained surface winds. These data are reported every 6 h for the life of the TC, and in some cases, are recorded when the system is classified as a non-TC (i.e., extratropical cyclone, Evans and Hart 2003; subtropical cyclone, Herbert and Poteat 1975; or tropical wave) to provide continuity over the life cycle of the disturbance. Those non-TCs are excluded from this study, as are any TCs with maximum sustained 1-min surface winds below 35 kt. The location of the TS, H, or IH genesis point defines the basin to which it belongs, even if it later crosses into another basin.

## 3. MJO analysis

### a. NOAA MJO index

For over four decades, it has been recognized that geophysical fields are often significantly correlated in both time and space. Empirical orthogonal function (EOF) analysis techniques (Kutzbach 1967; Barnett 1977) allow relatively simple descriptions of complex variations in these geophysical fields. Using observations and reanalysis data, several recent studies have developed MJO indices using EOF analyses (Lo and Hendon 2000; Higgins and Shi 2001; Hall et al. 2001; Y. Xue et al. 2002, personal communication; Wheeler and Hendon 2004). The NOAA Climate Prediction Center (CPC) currently maintains one such MJO composite index in real time (Y. Xue et al. 2002, personal communication) archived back to 1 January 1978. For this study, we focus on understanding both the statistical and



physical relationships between the MJO and TC activity, with a future goal of moving toward a real-time forecasting system. Thus, we will use the MJO composite of Y. Xue et al. (2002, personal communication) rather than redevelop existing indices.

Y. Xue et al. (2002, personal communication) applied extended empirical orthogonal function (EEOF; Weare and Nasstrom 1982) analysis to bandpass-filtered non-overlapping pentads (5-day means) of velocity potential at 200 hPa derived from the National Centers for Environmental Prediction (NCEP)–National Center for Atmospheric Research (NCAR) reanalysis data (Kalnay et al. 1996) during the November–April period from 1979 to 2000. To eliminate frequencies not germane to the MJO (e.g., Zhou and Miller 2005), they applied a 10- to 90-day bandpass filter, and to limit contamination of the signal by ENSO, they calculated the EEOFs from data during neutral and weak ENSO years. The first EEOF is composed of 10 time-lagged patterns and describes an eastward-propagating oscillation with zonal wavenumber 1 and a time scale of about 45 days. Velocity potential anomaly centers associated with the 10 time-lagged patterns were found to be centered at 10 unevenly spaced longitude locations: 80°E, 100°E, 120°E, 140°E, 160°E, 120°W, 40°W, 10°W, 20°E, and 70°E (see Fig. 2). Ten time series provide the amplitude and sign of each of these spatial patterns. The CPC archives the 10 MJO indices online at [http://www.cpc.ncep.noaa.gov/products/precip/CWlink/daily\\_mjo\\_index/proj\\_norm\\_order.ascii](http://www.cpc.ncep.noaa.gov/products/precip/CWlink/daily_mjo_index/proj_norm_order.ascii). These indices are the result of regressing the raw 200-hPa velocity potential anomalies onto the corresponding pattern of the first EEOF and then normalizing each index value by dividing it by its standard deviation. The zonal wavenumber 1 is clearly visible in the normalized velocity potential anomalies for the pentad 31 May–4 June 2005 (Fig. 3). Positive velocity potential anomalies are found at MJO indices 8, 9, 10, 1, and 2, and negative anomalies are found at MJO indices 3 to 7. For a full description of the CPC MJO index and methodology see Y. Xue et al. (2002, personal communication) and the CPC Web site [http://www.cpc.ncep.noaa.gov/products/precip/CWlink/daily\\_mjo\\_index/mjo\\_index.shtml](http://www.cpc.ncep.noaa.gov/products/precip/CWlink/daily_mjo_index/mjo_index.shtml). Because the 10 indices are themselves derived from the same EEOF analysis, we will, without loss of generality, present results from 2 of the 10 indices: index 1, calculated from equatorial velocity potential anomalies along 80°E, and index 6, calculated along 120°W. As noted in section 4, indices 1 and 6 are often similar in magnitude but opposite in sign, confirming the wavenumber (1) of the MJO. To demonstrate the phenomenon from indices in quadrature, one example using index 8, calculated along

10°W, and index 10, calculated along 70°E, (a difference of 80°) will also be presented in section 4.

MJO indices 1, 6, 8, and 10 were each divided into three phases for this study: negative (NEG), defined as any standardized velocity potential anomaly equal to or lower than  $-1.0$ ; neutral (NEU), defined as any standardized velocity potential anomaly between  $-1.0$  and  $+1.0$ ; and positive (POS), defined as any standardized velocity potential anomaly greater than or equal to  $+1.0$ . These break points were chosen to represent velocity potential anomalies more than one standard deviation from the mean.

### b. Velocity potential

Velocity potential  $\chi$ , mathematically represented as the inverse Laplacian of the gradient of the three-dimensional irrotational wind (Mancuso 1967), has been used extensively as an effective diagnostic of large-scale mass circulation. Chen et al. (1999), in their Eqs. (2)–(4), expressed velocity potential as a function of diabatic heating and thermal temperature advection, and concluded the “divergent circulation of both the long- and short-wave regimes are primarily maintained by diabatic heating” in the tropics. Rasmusson and Mo (1993) found strong agreement between centers of velocity potential anomalies and OLR and used velocity potential to diagnose convergence anomalies in the Hadley and Walker cell circulations both in the tropics and extratropics. Furthermore, Knutson and Weickmann (1987) undertook an extensive analysis of the MJO using 250-hPa velocity potential and found that “large-scale divergence (negative velocity potential) anomalies at upper-levels are usually accompanied by large-scale convergence (positive velocity potential) anomalies at lower levels, with large-scale rising motion in the intermediate levels” (Knutson and Weickmann 1987). Thus, synoptic-scale upper-tropospheric divergence (convergence) is strongly connected to negative (positive) velocity potential anomalies and with enhancement (suppression) of large-scale rising motion. These conditions have been identified as critical to tropical cyclogenesis and intensification (Gray 1968). Thus, while maximum (minimum) values of velocity potential may not correspond exactly to centers of upper-tropospheric convergence (divergence), we believe the relationships are sufficiently well-documented to connect the MJO’s modification of the upper troposphere to TC activity. This physical relationship, which forms the basis of our interpretation, will be discussed more in section 5.

### c. Hypothesis tests

We tested the statistical significance of MJO modulation of four types (events) of TC activity: tropical

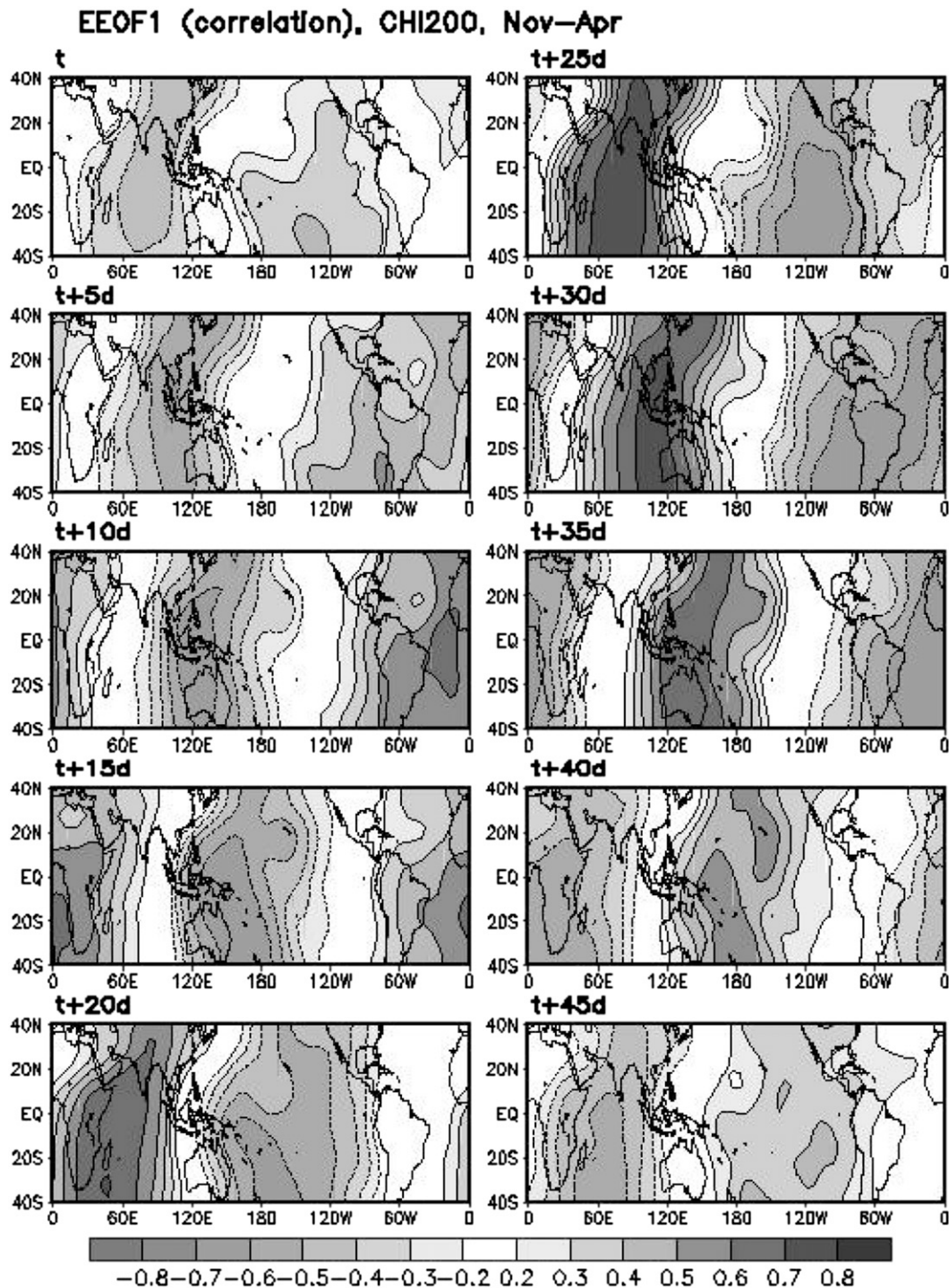


FIG. 2. The 10 MJO patterns of the first empirical orthogonal function of 200-hPa velocity potential: (upper left) day 0 ( $t$ ), (lower left) time progresses every five days, to day 20 ( $t + 20$  d), (upper right) day 25 ( $t + 25$  d), and (lower right) day 45 ( $t + 45$  d). Positive correlations (solid contours) correspond to suppressed 200-hPa convergence; negative correlations (dashed contours) correspond to 200-hPa divergence. Here the top two panels have strong divergence (convergence) centered over  $100^{\circ}\text{E}$ , which progress eastward in the lower panels (adapted from Y. Xue et al. 2002, personal communication).

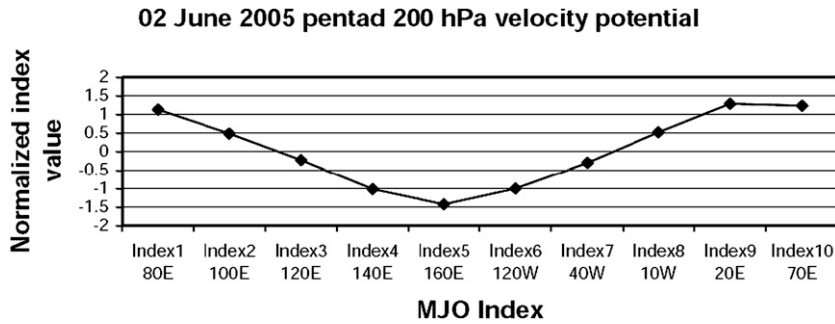


FIG. 3. MJO indices from 2 Jun 2005. Positive (negative) index values indicate positive (negative) velocity potential anomalies. The zonal wavenumber-1 oscillation is easily noticeable, with the maximum positive velocity potential anomaly located at 20°E and the minimum negative anomaly located at 160°E.

storm genesis, hurricane genesis, intense hurricane genesis, and landfall (LF). The yearday of each event was matched with its corresponding pentad MJO index, and thus was associated with an MJO phase. We tested the hypothesis that TC activity is uniformly distributed across MJO phase. The null,  $H_0$ , and alternative,  $H_A$ , hypotheses are therefore:

$$\begin{aligned} H_0 : \hat{p} &= p_0 \quad \text{and} \\ H_A : \hat{p} &\neq p_0, \end{aligned} \tag{1}$$

where  $\hat{p}$  and  $p_0$  are the observed and expected fraction of TC activity for each MJO phase. The observed fraction is calculated by dividing the number of TS, H, IH, and LF events during each MJO phase by the total number of TS, H, IH, and LF events across all MJO phases. The expected fraction of TC activity is simply the frequency of each MJO phase. The null hypothesis implies that there is no modulation of TC activity by the MJO and the alternative hypothesis implies that TC activity is modulated by the MJO. Coincident with this null hypothesis, the probability of cyclogenesis was assumed to be fixed, leading to a binomial distribution (e.g., Hall et al. 2001; Bessafi and Wheeler 2006). The relevant test statistic for each of the 10 MJO indices is given by:

$$Z_{\text{basin, storm\_type, MJO\_phase}} = \frac{\hat{p}_{\text{basin, storm\_type, MJO\_phase}} - p_{0\text{MJO\_phase}}}{\sqrt{p_{0\text{MJO\_phase}}(1 - p_{0\text{MJO\_phase}})/N_{\text{storm\_type}}}}, \tag{2}$$

where  $N$  is the total number of TC events in each category, basin is determined by the point of genesis, storm\_type is TS, H, IH, or LF, and MJO\_phase is NEG, NEU, or POS. The test statistic measures the statistical significance of the difference between observed and expected levels of TC activity, and the critical  $Z$  statistic at the 95% confidence level is  $\pm 1.96$ . The

null hypothesis can be rejected in favor of the alternative hypothesis, with 95% confidence, for  $Z$  statistics that exceed the critical  $Z$ , and each rejection indicates a statistically significant modulation of TC activity by the MJO. Finally, positive  $Z$  statistics indicate that more TC activity occurred than was expected, and likewise, negative  $Z$  statistics indicate that less TC activity occurred than was expected.

d. Wavelet analysis

Wavelet analysis is a powerful tool for determining the dominant modes of variability of a time series (Torrence and Compo 1998). The Morlet wavelet transform was used in this study to decompose time series of daily ACE into time–frequency space. The Morlet wavelet consists of a plane wave multiplied by a Gaussian function:

$$\psi_0(\eta) = \pi^{-1/4} e^{i\omega_0\eta} e^{-\eta^2/2}, \tag{3}$$

where  $\omega_0$  is the nondimensional frequency and  $\eta$  is a nondimensional time parameter. The wavelet has zero mean and is localized in both time and frequency space (Farge 1992; Torrence and Compo 1998). This particular technique is applicable because the time series of ACE contains nonstationary power at multiple frequencies (Daubechies 1990). To minimize the errors near the beginning and end of the wavelet power spectrum due to using finite-length datasets, the time series is padded with sufficient zeros to bring the total length up to the next-highest power of 2. While this padding serves to both limit edge effects and speeds up the Fourier transform, the added zeros reduce cyclic continuity and could introduce spurious amplitude in the power spectrum at the edges. However, because TC activity is infrequent in the first and last days of each year, the padded time series will not significantly

TABLE 2. The TC activity events per phase (NEG, NEU, or POS) of MJO index 1, defined as 200-hPa velocity potential at 80°E, for the period 1978–2006. Observed  $\hat{p}$  and expected  $p_0$  (see Table 4 for expected values) levels of TS, H, and IH genesis activity are used to compute the relevant  $Z$  statistic in (2). Critical  $Z$  at the 95% confidence level is  $\pm 1.96$ ; boldface indicates significance at this level. Negative  $Z$  statistics indicate fewer events occurred than expected and positive statistics indicate more events occurred than expected.

Index 1			CPAC	WEPAC	CEPAC	EEPAC	EPAC	NATL	GOM	CARIB	AMDR
TS	NEG	OBS	3	5	32	5	45	72	16	15	44
		Z stat	-0.72	<b>-2.34</b>	<b>-2.27</b>	-1.55	<b>-3.52</b>	<b>3.55</b>	<b>2.14</b>	<b>2.60</b>	<b>4.43</b>
	NEU	OBS	16	60	224	45	345	223	43	37	100
		Z stat	<b>-2.11</b>	-0.24	0.23	0.00	-0.43	-1.61	-1.17	-0.67	<b>-2.75</b>
	POS	OBS	10	19	50	12	91	30	6	2	15
		Z stat	<b>3.46</b>	<b>2.88</b>	<b>2.16</b>	1.69	<b>4.43</b>	-1.68	-0.75	-1.92	-1.10
H	NEG	OBS	1	6	16	0	23	42	6	9	22
		Z stat	-0.91	-1.32	<b>-2.28</b>	-1.46	<b>-3.02</b>	<b>2.96</b>	0.84	<b>2.17</b>	<b>3.37</b>
	NEU	OBS	11	51	133	10	205	130	21	22	51
		Z stat	0.06	1.06	0.63	0.83	1.22	-0.48	-0.02	-0.20	-1.08
	POS	OBS	3	8	29	2	42	11	2	0	3
		Z stat	0.91	0.00	1.63	0.46	1.63	<b>-2.59</b>	-0.88	<b>-2.08</b>	<b>-2.21</b>
IH	NEG	OBS	2	3	11	0	16	20	1	5	9
		Z stat	0.03	-1.39	-0.25	-0.42	-0.99	<b>2.93</b>	-0.75	1.36	1.95
	NEU	OBS	9	30	58	0	97	50	11	14	24
		Z stat	-0.27	0.08	0.35	-1.63	0.08	-0.79	0.97	0.11	0.02
	POS	OBS	2	8	9	1	20	3	1	0	0
		Z stat	0.34	1.41	-0.20	<b>2.67</b>	0.97	<b>-2.13</b>	-0.50	-1.63	<b>-2.15</b>

influence the amplitude of the power spectra. Statistical significance of the wavelet power spectrum is determined using the method of Torrence and Compo (1998), multiplying the Fourier power spectrum [their Eq. (16)] by the chosen percentile value for  $\chi^2_2$  (a chi-square distribution with 2 degrees of freedom).

#### 4. Results

To statistically quantify the modulation of TC activity by the MJO, 1710 hypothesis tests were performed in

this study. For each basin and subbasin, we were able to reject null hypotheses in favor of alternative hypotheses, thereby confirming a statistically significant modulation of TC activity by the MJO over the entire Western Hemisphere. As discussed in section 3, we present a representative sample of results from MJO indices 1 and 6 without loss of generality, as all 10 indices are derived from the same EEOF. Additionally, because they are often opposite in sign but similar in magnitude, and are separated by 160° longitude, these two indices confirm the wavenumber-1 nature of the

TABLE 3. As in Table 2, but for MJO index 6.

Index 6			CPAC	WEPAC	CEPAC	EEPAC	EPAC	NATL	GOM	CARIB	AMDR
TS	NEG	Obs	9	19	50	12	90	23	5	1	11
		Z stat	<b>3.23</b>	<b>3.10</b>	<b>2.51</b>	1.87	<b>4.76</b>	<b>-2.61</b>	-1.01	<b>-2.26</b>	-1.88
	NEU	Obs	17	60	222	43	342	236	47	42	106
		Z stat	-1.78	-0.38	-0.28	-0.70	-1.07	-0.26	-0.17	0.75	-1.88
	POS	Obs	3	5	34	7	49	66	13	11	42
		Z stat	-0.70	<b>-2.32</b>	-1.91	-0.82	<b>-2.96</b>	<b>2.67</b>	1.13	1.10	<b>4.03</b>
H	NEG	Obs	2	8	30	3	43	7	2	0	2
		Z stat	0.19	0.15	<b>2.13</b>	1.43	<b>2.14</b>	<b>-3.32</b>	-0.81	<b>-2.03</b>	<b>-2.46</b>
	NEU	Obs	12	50	132	7	201	136	21	21	53
		Z stat	0.59	0.67	0.27	-1.17	0.44	0.32	-0.10	-0.69	-0.69
	POS	Obs	1	7	16	2	26	40	6	10	21
		Z stat	-0.90	-0.96	<b>-2.25</b>	0.16	<b>-2.48</b>	<b>2.59</b>	0.86	<b>2.69</b>	<b>3.08</b>
IH	NEG	Obs	1	8	9	1	19	2	1	0	0
		Z stat	-0.45	1.55	-0.05	<b>2.74</b>	0.92	<b>-2.39</b>	-0.45	-1.59	<b>-2.09</b>
	NEU	Obs	10	29	58	0	97	50	10	13	23
		Z stat	0.30	-0.37	0.22	-1.66	-0.09	-0.92	0.30	-0.48	-0.46
	POS	Obs	2	4	11	0	17	21	2	6	10
		Z stat	0.04	-0.94	-0.22	-0.42	-0.72	<b>3.29</b>	0.04	<b>2.02</b>	<b>2.46</b>



TABLE 4. Expected fraction of TC activity  $p_0$  determined by the frequency of each MJO phase per index. For this study, only results from MJO indices 1 and 6 (highlighted in boldface type) are presented without loss of generality because all 10 indices are derived from the same EEOF.

MJO index	Total pentads	Pentads NEG	Fraction NEG	Pentads NEU	Fraction NEU	Pentads POS	Fraction POS
<b>Index 1</b>	<b>1066</b>	<b>161</b>	<b>0.15</b>	<b>774</b>	<b>0.73</b>	<b>131</b>	<b>0.12</b>
Index 2	1066	169	0.16	775	0.73	122	0.11
Index 3	1066	172	0.16	771	0.72	123	0.12
Index 4	1066	175	0.16	738	0.69	153	0.14
Index 5	1066	144	0.14	764	0.72	158	0.15
<b>Index 6</b>	<b>1066</b>	<b>125</b>	<b>0.12</b>	<b>781</b>	<b>0.73</b>	<b>160</b>	<b>0.15</b>
Index 7	1066	117	0.11	784	0.74	165	0.15
Index 8	1066	133	0.12	766	0.72	167	0.16
Index 9	1066	159	0.15	760	0.71	147	0.14
Index 10	1066	165	0.15	769	0.72	132	0.12

oscillation. Furthermore, to illustrate the modulations from indices in quadrature, one example using indices 8 and 10 is presented. It is a simple matter to repeat our analyses using other pairs of indices.

*a. Tropical storms*

In each of the nine basins, TS genesis activity was found to be statistically significantly modulated by the MJO, and statistics from the EPAC basin are presented here as a representative sample. When index 1 was in

the POS phase and index 6 in the NEG phase, 91 and 90 TSs, respectively, formed in the EPAC, out of 481 total, corresponding to observed fractions  $\hat{p}$  of 0.19 and 0.19 (Tables 2–3). Comparing the observed fractions with the expected fractions  $p_0$  of 0.12 and 0.12, respectively (Table 4) results in  $Z$  statistics of 4.43 and 4.76, which are both statistically significant at the 95% confidence level. Furthermore, approximately 50% fewer TSs formed in the EPAC when indices 1 and 6 reversed phases, corresponding to  $Z$  statistics of  $-3.52$  and

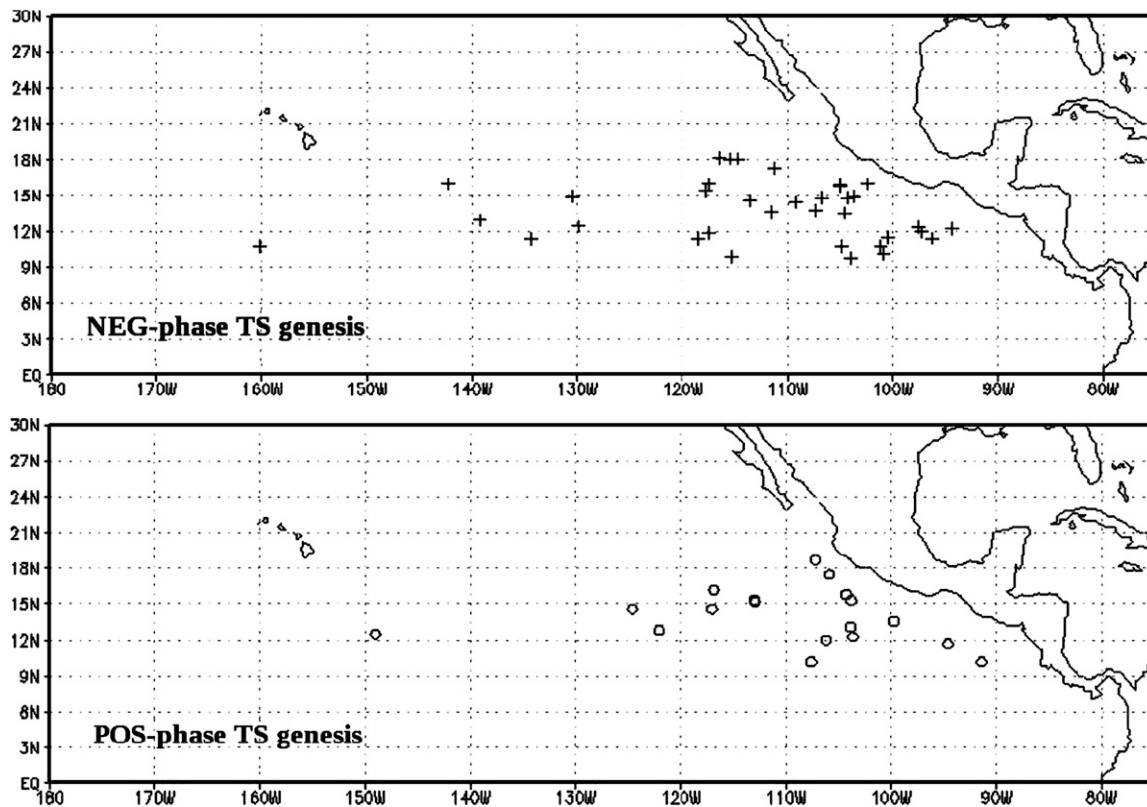


FIG. 4. The TS genesis points for the EPAC stratified by phase of MJO index 6. Open circles (crosses) are points of TS genesis for the POS (NEG) phase. NEU-phase genesis points are omitted, and every fifth point is plotted to simplify the figure.

TABLE 5. Summary of modulation of TC activity as measured by TS genesis events by MJO indices 1 and 6. “More” and “less likely” are defined as an exceedance of the critical Z statistic at the 95% confidence level and are highlighted in boldface. Similar conclusions for H and IH genesis events (not shown) are easily identifiable from Tables 2–3.

Basin	Phase of MJO index 1		
	NEG	NEU	POS
CPAC	None	<b>Less likely</b>	<b>More likely</b>
WEPAC	<b>Less likely</b>	None	<b>More likely</b>
CEPAC	<b>Less likely</b>	None	<b>More likely</b>
EEPAC	None	None	None
EPAC	<b>Less likely</b>	None	<b>More likely</b>
NATL	<b>More likely</b>	None	None
GOM	<b>More likely</b>	None	None
CARIB	<b>More likely</b>	None	None
AMDR	<b>More likely</b>	<b>Less likely</b>	None

Basin	Phase of MJO index 6		
	NEG	NEU	POS
CPAC	<b>More likely</b>	None	None
WEPAC	<b>More likely</b>	None	<b>Less likely</b>
CEPAC	<b>More likely</b>	None	None
EEPAC	None	None	None
EPAC	<b>More likely</b>	None	<b>Less likely</b>
NATL	<b>Less likely</b>	None	<b>More likely</b>
GOM	None	None	None
CARIB	<b>Less likely</b>	None	None
AMDR	None	None	<b>More likely</b>

–2.96. Figure 4 shows the distribution of TS genesis points for the EPAC for the period 1978–2006 stratified by phase of MJO index 6. Every fifth genesis point is plotted to simplify the figure, and NEU-phase genesis points, which do not have statistical significance for the EPAC, are omitted. In addition to the overall reduction in TS genesis activity across the entire EPAC during the

POS phase of index 6, there is a marked decline in activity west of about 120°W. This modulation is statistically significant for the CEPAC, WEPAC, and CPAC subbasins (Tables 2–3). Thus TS genesis was statistically significantly favored in the EPAC when index 1 (index 6) was in the POS (NEG) phase, and cyclogenesis was not favored when index 6 (index 1) was in the NEG (POS) phase. Table 5 summarizes the interpretation of TS genesis for each of the nine basins and subbasins.

In addition to examining the modulation of EPAC TS genesis by the MJO through indices 1 and 6, it is also possible, by examining the variations of one index from west to east, to demonstrate the zonal and temporal character of the oscillation. Figure 5 presents Z statistics from the CPAC eastward to the AMDR (a distance of almost 10 000 km) for index 1. The modulation during NEG phase begins weakly in the CPAC, quickly becomes statistically significant in the WEPAC and CEPAC, and then diminishes in magnitude in the EEPAC. Crossing Central America, the NEG modulation reverses signs in the GOM and CARIB, and again becomes statistically significant (with the opposite sign) in the AMDR. A similar, but opposite, pattern emerges with the modulation during POS phase. The NEU phase is insignificant for all basins except the CPAC and AMDR, where significantly fewer TSs form during the NEU phase. The pattern displayed in Fig. 5 is interpreted as follows: when index 1 is in POS phase, significantly more TSs form in the CPAC, WEPAC, and CEPAC; and significantly fewer TSs form in the CARIB. When index 1 is in NEG phase, significantly fewer TSs form in the WEPAC and CEPAC, and significantly more TSs form in the GOM, CARIB, and AMDR. This pattern confirms the wavenumber-1 character of the MJO, and shows how the behavior of the modulation changes with time and

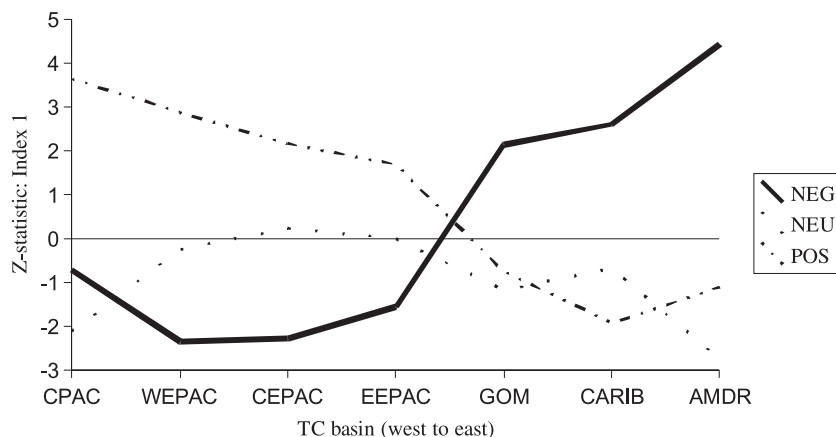


FIG. 5. The Z statistics for three phases of index 1 from the CPAC eastward to the AMDR. The reversal of sign in the modulations from left to right for both POS and NEG phases shows the MJO wavenumber 1.

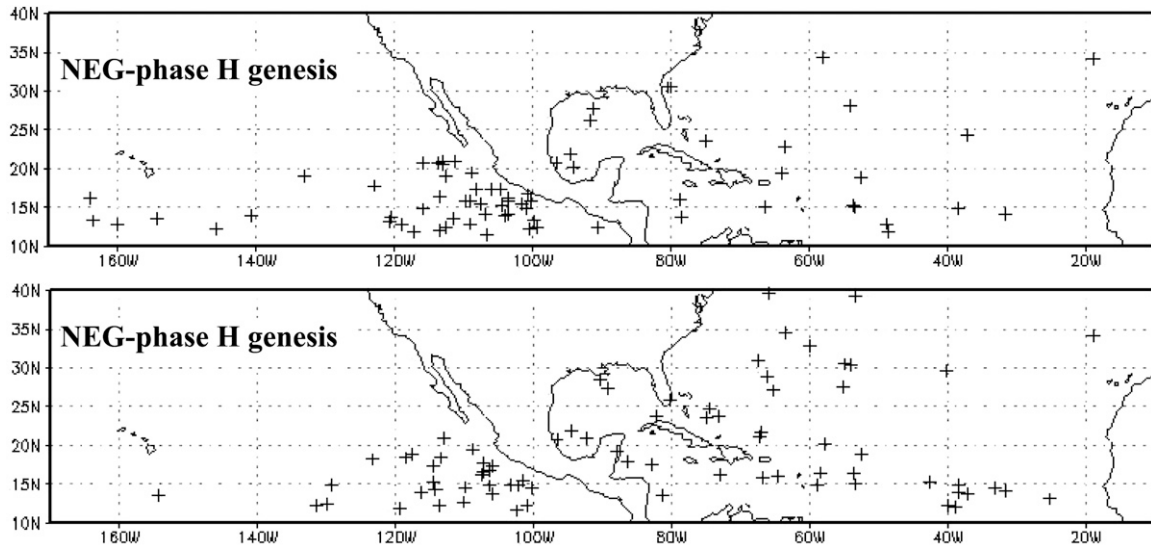


FIG. 6. The H genesis points for the EPAC and NATL for MJO (top) index 8 and (bottom) index 10, both in NEG phase. Quadrature of the indices is evident as mean distribution of genesis points moves west (in top panel) to east (in bottom panel) with MJO.

eastward progress. A similar analysis from index 7 (not shown) confirms that the eastward-propagating MJO first affects the western portion of the EPAC and then continues into the NATL. This characteristic is clearly demonstrated by MJO indices 8 and 10, which are in near quadrature (Fig. 6): when index 8 was NEG, H genesis points concentrated in the EPAC; however, when index 10 was NEG, the concentration shifted eastward into the NATL. Furthermore, favorable conditions for TC genesis in the EPAC are often out of phase with favorable conditions in the NATL, suggesting the presence of an EPAC–NATL dipole in TC activity. This feature is discussed further in section 5a.

#### b. Hurricanes

For this subsection, statistics from the CEPAC subbasin are presented as a representative sample to highlight the MJO modulation of H activity. When index 1 was in the POS phase and index 6 was in the NEG phase; 29 and 30 hurricanes formed, respectively, in the CEPAC, out of 178 total, corresponding to observed fractions  $\hat{p}$  of 0.16 and 0.17 (Tables 2–3). Comparing the observed fractions with the expected fractions  $p_0$  of 0.15 and 0.15, respectively (Table 4) results in  $Z$  statistics of 1.63 and 2.13, with the latter statistically significant at the 95% confidence level. Similar to the modulation of TS genesis in the EPAC, approximately 50% fewer hurricanes formed in the CEPAC when index 1 (index 6) was in the NEG (POS) phase, 16 and 16 Hs, respectively, corresponding to  $Z$  statistics of  $-2.28$  and  $-2.25$ . Figure 7 shows the dis-

tribution of H genesis points during positive and negative phases of MJO index 1 for the CEPAC for the period 1978–2006. Tables 2–3 summarize observed levels and  $Z$  statistics for H activity in all nine basins and subbasins.

#### c. Intense hurricanes

To highlight the MJO modulation of IH activity, statistics from the AMDR subbasin are presented. When index 1 was in the NEG phase and index 6 was in the POS phase, 9 and 10 IHs formed, respectively, in the AMDR, out of 33 total, corresponding to observed fractions  $\hat{p}$  of 0.27 and 0.30, respectively (Tables 2–3). Comparing the observed fractions with the expected fractions  $p_0$  of 0.15 and 0.15 (Table 4) results in  $Z$  statistics of 1.95 and 2.46, with the latter statistically significant at the 95% confidence level. No IHs formed in the AMDR when index 1 (index 6) was in the NEG (POS), giving  $Z$  statistics of  $-2.15$  and  $-2.09$ , respectively. Thus IH genesis was statistically significantly favored in the AMDR when index 1 (index 6) was in the NEG (POS) phase, and genesis was not favored when index 1 (index 6) was in the NEG (POS) phase. Figure 8 shows the distribution of IH genesis points for the AMDR for 1978–2006 during positive and negative phases of MJO index 6.

#### d. Landfall

Here the NATL basin is examined to quantify the MJO modulation of TC landfalls. Unlike the previous

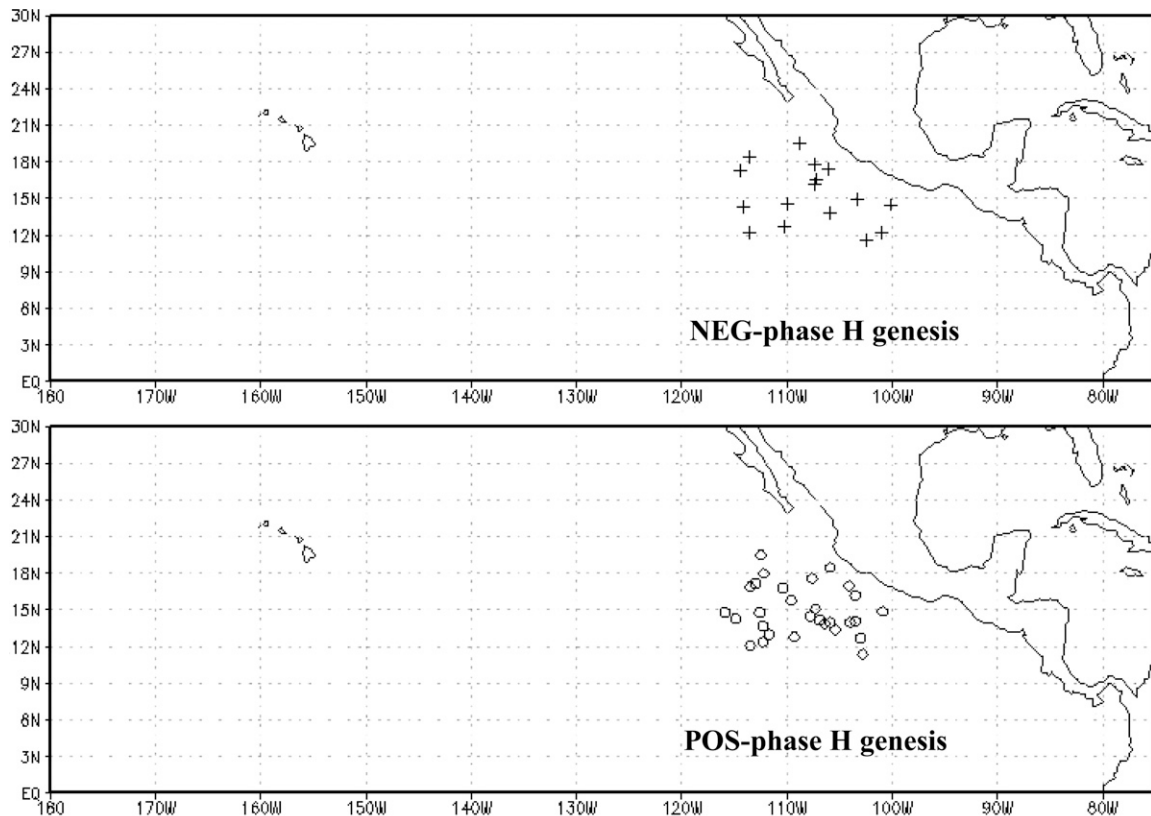


FIG. 7. The H genesis points for the CEPAC stratified by phase of MJO index 1. Open circles (crosses) are points of H genesis for the POS (NEG) phase. NEU-phase genesis points are omitted.

subsections, for TC activity defined by landfall, we only examined the NATL basin because of the lack of temporal data in the landfall records for the EPAC. For this series of hypothesis tests, we define “landfall” to include TCs whose centers came within 100 km of a coastline (e.g., Powell and Aberson 2001), and we match the Julian date of landfall with its corresponding MJO index. When index 1 was in NEG phase, 24 out of 83 Hs made landfall and 13 out of 61 IHs made landfall (Fig. 9), corresponding to  $Z$  statistics of 3.51 and 1.35, respectively (Table 6). The ratio of H and IH landfalls is 37 to 9, or 4 to 1, when comparing phases of index 1. Furthermore, no H or IH made landfall equatorward of 20°N when index 6 was in NEG phase (not shown), a statistic very important to the vulnerable countries surrounding the Caribbean Sea. Finally, when both indices 1 and 6 were in the NEU phase (one of the few tests to show any statistically significant relationship to the NEU phase), fewer Hs made landfall: only 50 (49) made landfall when index 1 (index 6) was NEU. Table 6 summarizes the observed levels and  $Z$  statistics for landfall activity across the NATL for both MJO indices.

#### e. Wavelet analysis of ACE

A detailed Morlet wavelet analysis was carried out on daily values of accumulated cyclone energy (ACE) for the EPAC and NATL basins for the period 1970–2006. Peaks in the power spectra of ACE occurred between 30 and 50 days (Fig. 10) in both the EPAC and NATL basins. These peaks in the power spectra are relatively small, and border on statistical significance (the dashed curve plots 90% significance, which asymptotes quickly beyond 90 days because of the strong annual cycle present in ACE data). However, we believe they provide valuable indirect evidence supporting the modulation of TC activity by the MJO, especially given that no other major atmospheric mode operates on the time scale of the MJO. Furthermore, several factors may limit the magnitude and thus the statistical significance of the spectral peaks. First, ACE is highly sensitive to strong or long-lasting TCs. For example, one IH with maximum sustained winds of 100 kt lasting for only 1 day can mask the ACE signal of a 45-kt TC lasting 5 days. Second, ACE, as a metric that sums squares of maximum wind speed, is particularly sensitive to the



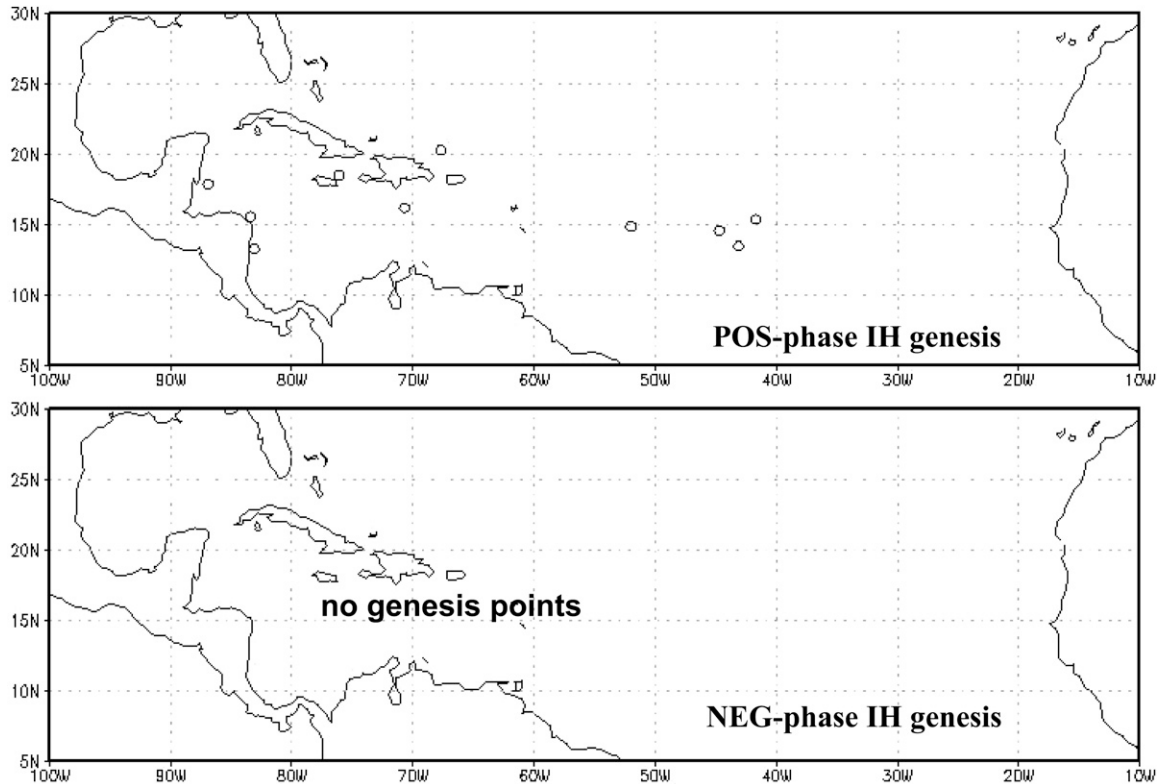


FIG. 8. The IH genesis points for the AMDR stratified by phase of MJO index 6. Open circles are points of IH genesis for the POS phase. No IHs formed in the AMDR during the NEG phase of MJO 6. NEU-phase genesis points are omitted.

flaws in the best-track data referenced in section 2. Alternative metrics, including the power dissipation index (PDI; Emanuel 2005) and scaled TC-day index (Jury et al. 1999) have been proposed, but these metrics are also not without flaws. Third, major changes in operational practice and observing technology have occurred in the EPAC and NATL over the period 1970–2006, and these changes have likely impacted the best-track record (e.g., Buckley et al. 2003; Landsea 2007). However, despite these limitations, the power spectra peaks correspond closely with the time scale of the MJO, and are nearly statistically significant at the 90% confidence level. Thus, this wavelet analysis serves as an indirect, but important, confirmation of the modulation of the MJO on TC activity, as measured by ACE, in the EPAC and NATL basins.

#### f. Seasonal prediction

In addition to its value in intraseasonal modulation of TC activity, we found evidence that the MJO may also be an important predictor of TC activity on the seasonal time scale (e.g., Wheeler and Weickmann 2001). For example, for the NATL basin, TS, H, and IH activity are all more likely when MJO index 6 is in the POS phase

(Table 3), defined as positive 200-hPa velocity potential anomalies at 120°W. During the very active 2005 North Atlantic season, index 6 averaged 0.32 from June to November, a significant departure from the expected seasonal mean of 0.00. For comparison, in 2004 and 2006, index 6 averaged 0.01 and  $-0.03$ , respectively, during the same period. While choice of averaging interval affects the mean value, similar mean values were found from June to October (0.38) and from May to November (0.26). Thus, given that intraseasonal predictability of the MJO is improving (e.g., Mo 2001; Hendon et al. 2000; Inness and Slingo 2003; Jones et al. 2004; Reichler and Roads 2005; Vitart et al. 2007; Hendon et al. 2007), we suggest future studies examine the effectiveness of expected MJO phase as a predictor of seasonal levels of TC activity, both for the nine basins examined in this study and for other global TC basins.

## 5. Discussion

### a. Pacific–Atlantic dipole

Through an extensive series of hypothesis tests, we have quantified the modulations over nine regions of the Western Hemisphere. MJO indices 1 and 6, which are located 160° apart (at 80°E and 120°W), were often

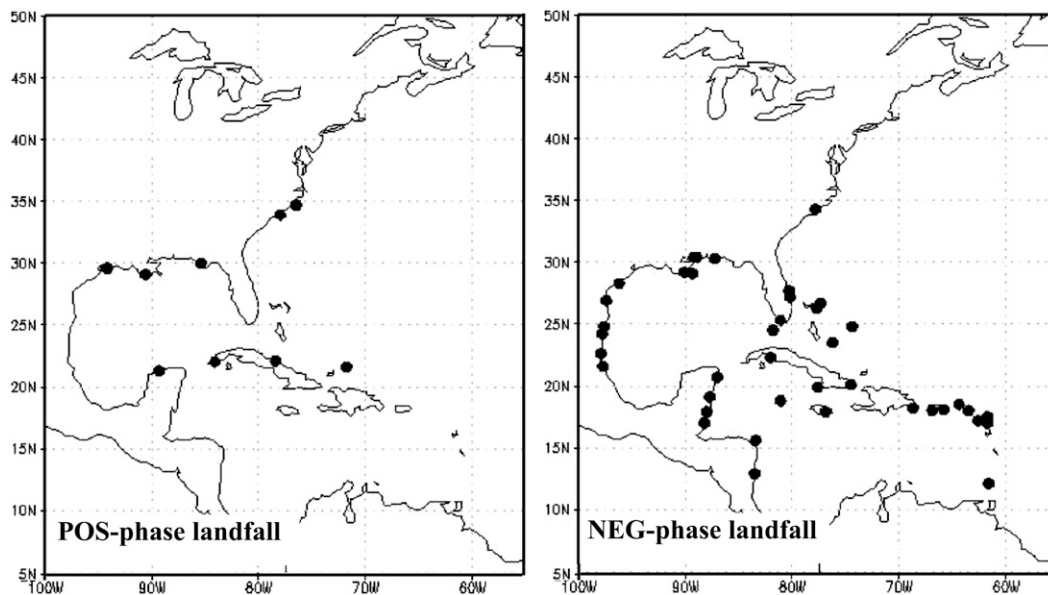


FIG. 9. Landfall points for the NATL stratified by phase of MJO index 1. Closed circles are points of H and IH landfall; also shown is (left) landfall during POS phase, and (right) landfall during NEG phase. NEU-phase landfall points are omitted.

similar in magnitude but opposite in sign, highlighting the zonal wavenumber 1 of the MJO. Spatially, this dipole can be seen as opposing signals between the CPAC (westernmost) and AMDR (easternmost) sub-basins. For example, when H formation was favored in the CPAC, it was not favored in the AMDR. The same patterns were also noticeable between the NATL and EPAC, despite their much broader longitudinal extent. For example, TS, H, and IH formation were all strongly favored in the NATL when index 1 was in NEG phase, but TS and H formation was strongly suppressed in the EPAC during the same phase. These spatial patterns in the MJO modulation are also present from west to east in the  $Z$  statistics. West to east, the  $Z$  statistics for MJO index 6 modulation of TS genesis swing from very strongly positive to strongly negative, from 3.23, 3.10, 2.51, 1.87,  $-1.01$ ,  $-2.26$ , to  $-1.88$  for the CPAC, WEPAC, CEPAC, EEPAC, GOM, CARIB, and AMDR, respectively. This dipole suggests that a relationship exists between TC activity in the northeast Pacific and North Atlantic. For physical insight into this relationship, we examine the 200-hPa velocity potential.

#### b. Lower-tropospheric modulations

A large majority of TCs in the eastern hemisphere form in association with the monsoon trough (MT), a broad region of active convection in the Indian and west Pacific basins. In the Indian and west Pacific basins, the MJO signal shows up strongly in OLR data, and en-

hanced (suppressed) OLR indicates a more (less) active MT and thus favorable (unfavorable) local conditions for TC activity. In contrast, however, more than half of TCs in the North Atlantic generate from tropical easterly waves, and in this region there is no discernible in situ MJO signal in OLR data (Madden and Julian 1994). The process of cyclogenesis from tropical easterly waves is slower than cyclogenesis from the monsoon trough (Frank and Roundy 2006), suggesting a need for any MJO atmospheric modulation to occur over a broad spatial and temporal area.

TABLE 6. NATL TC landfall events per MJO index phase, 1978–2006. Critical  $Z$  at the 95% confidence level is  $\pm 1.96$ ; boldface indicates significance at this level. Negative  $Z$  statistics indicate fewer events occurred than expected and positive statistics indicate more events occurred than expected.

NATL landfall		Index 1		Index 6		Total no.
		80°E		120°W		
Storm type	MJO phase	Obs	$Z$ statistic	Obs	$Z$ statistic	
TC	NEG	26	1.82	4	<b>-2.94</b>	124
	NEU	92	0.40	96	1.05	
	POS	6	<b>-2.53</b>	24	1.35	
H	NEG	24	<b>3.51</b>	8	$-0.59$	83
	NEU	50	<b>-2.53</b>	49	<b>-2.93</b>	
	POS	9	$-0.40$	26	<b>4.16</b>	
IH	NEG	13	1.35	1	<b>-2.45</b>	61
	NEU	48	1.06	45	0.09	
	POS	0	<b>-2.92</b>	15	<b>2.10</b>	

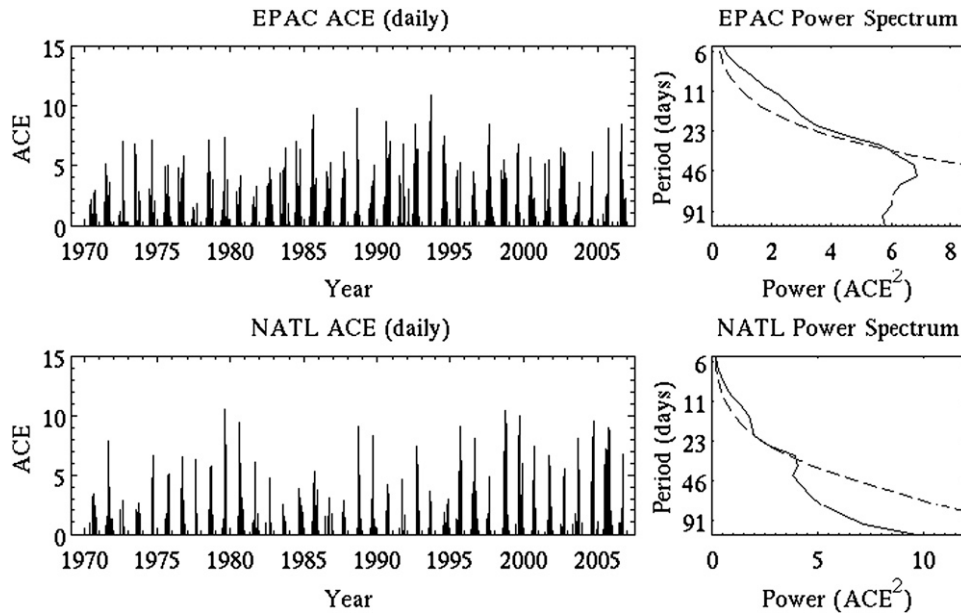


FIG. 10. Wavelet analysis of (top) EPAC and (bottom) NATL ACE. Also shown is the (left) time series of ACE and (right) power spectra analyses. Statistical significance at the 90% confidence level is indicated by the dashed curve. Peaks in the power spectra on the time scale of the MJO are found in both basins between 30 and 50 days.

Many studies (e.g., Madden and Julian 1994; Harr and Elsberry 1995; Wheeler and Hendon 2004; Arguez et al. 2005; Kiladis et al. 2005) have observed that the MJO typically completes its global circuit in the upper troposphere. Other studies have documented continuous low-level MJO propagation in 1000-hPa divergence (e.g., Hendon and Salby 1994), sea level pressure (e.g., Milliff and Madden 1996; Matthews 2000), and low-level humidity (e.g., Kiladis et al. 2005). As deep convection builds over the Maritime Continent, an west-east MJO teleconnection develops, identified as a Kelvin wave by Hendon and Salby (1994), and we believe this rapid, eastward-propagating Kelvin response to the MJO is responsible for the modulations in 200-hPa velocity potential. Accordingly, between the Americas and West Africa, we propose that smaller-scale lower-tropospheric environmental modulations, including 850-hPa wind anomalies, changes in low-level relative vorticity and low-level horizontal shear, and sea surface temperatures, are thus responses to synoptic- and planetary-scale forcing from the aforementioned eastward-propagating Kelvin wave. This hypothesis is in agreement with several of the studies discussed in section 1 (e.g., Molinari et al. 1997; Maloney and Hartmann 2000a,b; Collins and Mason 2000; Frank and Roundy 2006), who attributed modulation of TC activity to low-level circulation anomalies associated with the MJO as far east as the western Atlantic. Thus, over the Western

Hemisphere, it is likely that upper-tropospheric modulations act collectively with lower-tropospheric responses to promote or suppress tropical cyclogenesis.

### c. Physical interpretation: Genesis and intensification

As discussed in section 3b, the 200-hPa velocity potential is a measure of upper-tropospheric mass circulation, with regions of negative (positive) velocity potential associated with regions of upper divergence (convergence). Upper-tropospheric divergence, in addition to being one of the classic necessary conditions for TC development (Gray 1968), can also act to promote net column divergence (Gray 1979), which, by mass balance, acts to promote surface convergence. Thus, we propose the following the physical link between the MJO and TC activity: as the oscillation propagates eastward from the Maritime Continent and crosses the date line, it loses much of its lower-tropospheric signature. By the time it reaches the NATL basin, only the upper-tropospheric signal remains. However, when this component is strong (defined in this study as absolute values of velocity potential greater than one standard deviation from the mean), the eastward-propagating Kelvin wave modifies the large-scale environment, including through upper-tropospheric divergence (convergence), to promote conditions favorable (unfavorable) for tropical cyclogenesis at multiple spatial scales. This mechanism is directly supported by Madden and Julian

(1972, their Fig. 16) and is directly responsible for the dipole between Pacific and Atlantic TC activity quantified in this study.

#### *d. Physical interpretation: Atlantic landfall*

It follows that the physical mechanisms that explain the modulation of TC genesis and intensification might also be related to TC landfall. Enhancement of upper-tropospheric divergence promotes anticyclonic flow aloft, and we propose that when MJO phase favors TC genesis and intensification, it also modifies the large-scale environment to both promote genesis and also steer NATL TCs toward Central and North America. It is very likely that similar relationships exist between TC tracks and the MJO in other TC basins, including the west Pacific, Australian, and Indian basins, and indeed changes in TC track density because of shifting large-scale steering flows have been documented in the western North Pacific (Kim et al. 2008). Regional geography and oceanography, such as the presence of a continental landmass poleward of the mean TC trajectory, will also likely to affect the modulation. We will examine these relationships in more detail in a future study.

## 6. Conclusions

In this study, the role of the Madden–Julian oscillation was examined in modulating tropical cyclone activity in the North Atlantic basin, the northeast Pacific basin, and their associated subbasins for the period 1978–2006. Here, TC activity was defined as counts of genesis and landfall of tropical storms, hurricanes, and intense hurricanes, as well as by the integrative accumulated cyclone energy index. An operational MJO diagnostic derived from the 200-hPa velocity potential was divided into three phases and observed and expected levels of TC activity were compared using a binomial distribution hypothesis test. Because the MJO has a zonal wavenumber 1, it was sufficient to examine 200-hPa velocity potential at only one or two longitudinal locations and extrapolate the globally applicable metric to all basins. The major contributions of this study can be summarized as follows. 1) Statistically significant modulations of the frequency of TC genesis and intensification over nine basins from the central Pacific eastward to the North Atlantic were synthesized and quantified using an MJO metric valid for all the subbasins of the Western Hemisphere. 2) A dipole physically consistent with an eastward-propagating MJO event was found between TC activity in the western and eastern basins and subbasins. The TC landfall activity over the NATL was

found to be statistically significantly modulated by the MJO. 3) Upper-tropospheric divergence was proposed as the physical link between TC activity and the MJO. The eastward-propagating Kelvin wave sequentially modulates large-scale upper-tropospheric conditions, which impact TC genesis and intensification, and for the NATL basin, landfall.

Finally, it is noted that other MJO indices, including the Wheeler and Hendon (2004) index discussed in section 1, have demonstrated success in intraseasonal prediction of TC activity in the Australian Basin. We believe that developing statistical relationships for these MJO indices for TC activity in the Western Hemisphere and, reciprocally, applying the index from this study in the Eastern Hemisphere, would extend our understanding of how, physically, MJO modulates TC activity. Furthermore, because of the significant hazards posed by landfalling TCs, we suggest that future studies give particular emphasis to track and landfall relationships for each TC basin.

*Acknowledgments.* The authors acknowledge the many constructive comments from two anonymous reviewers whose suggestions greatly improved the content and structure of this manuscript. This work was supported in part by the University of Oklahoma and by Woodside Petroleum, Ltd. Wavelet software was provided by C. Torrence and G. Compo and is available at <http://atoc.colorado.edu/research/wavelets/>.

## REFERENCES

- Arguez, A., M. A. Bourassa, and J. J. O'Brien, 2005: Detection of the MJO signal from QuikSCAT. *J. Atmos. Oceanic Technol.*, **22**, 1885–1894.
- Barnett, T. P., 1977: The principal time and space scales of the Pacific trade wind fields. *J. Atmos. Sci.*, **34**, 221–236.
- Barrett, B. S., L. M. Leslie, and B. H. Fiedler, 2006: An example of the value of strong climatological signals in tropical cyclone track forecasting: Hurricane Ivan (2004). *Mon. Wea. Rev.*, **134**, 1568–1577.
- Bell, G. D., and M. Chelliah, 2006: Leading tropical modes associated with interannual and multidecadal variations in seasonal North Atlantic hurricane activity. *J. Climate*, **19**, 590–612.
- , and Coauthors, 2000: Climate assessment for 1999. *Bull. Amer. Meteor. Soc.*, **81**, S1–S50.
- Bessafi, M., and M. C. Wheeler, 2006: Modulation of south Indian Ocean tropical cyclones by the Madden–Julian oscillation and convectively coupled equatorial waves. *Mon. Wea. Rev.*, **134**, 638–656.
- Buckley, B. W., L. M. Leslie, and M. S. Speer, 2003: The impact of observational technology on climate database quality: Tropical cyclones in the Tasman Sea. *J. Climate*, **16**, 2640–2645.
- Chan, J. C. L., 2005: The physics of tropical cyclone motion. *Annu. Rev. Fluid Mech.*, **37**, 99–128.
- Chen, T. C., S. P. Weng, and S. Schubert, 1999: Maintenance of austral summertime upper-tropospheric circulation over tropical



- South America: The Bolivian high–Nordeste low system. *J. Atmos. Sci.*, **56**, 2081–2100.
- Collins, J. M., and I. M. Mason, 2000: Local environmental conditions related to seasonal tropical cyclone activity in the Northeast Pacific basin. *Geophys. Res. Lett.*, **27**, 3881–3884.
- Daubechies, I., 1990: The wavelet transform, time-frequency localization and signal analysis. *IEEE Trans. Info. Theory*, **36**, 961–1005.
- Emanuel, K. A., 2005: Increasing destructiveness of tropical cyclones over the past 30 years. *Nature*, **436**, 686–688.
- , 2006: Climate and tropical cyclone activity: A new model downscaling approach. *J. Climate*, **19**, 4797–4802.
- , R. Sundararajan, and J. Williams, 2008: Hurricanes and global warming: Results from downscaling IPCC AR4 simulations. *Bull. Amer. Meteor. Soc.*, **89**, 347–367.
- Evans, J. L., and R. E. Hart, 2003: Objective indicators of the life cycle evolution of extratropical transition for Atlantic tropical cyclones. *Mon. Wea. Rev.*, **131**, 909–925.
- Farge, M., 1992: Wavelet transforms and their applications to turbulence. *Annu. Rev. Fluid Mech.*, **24**, 395–457.
- Frank, W. M., and P. E. Roundy, 2006: The role of tropical waves in tropical cyclogenesis. *Mon. Wea. Rev.*, **134**, 2397–2417.
- , and G. S. Young, 2007: The interannual variability of tropical cyclones. *Mon. Wea. Rev.*, **135**, 3587–3598.
- Franklin, J. L., C. J. McAdie, and M. B. Lawrence, 2003: Trends in track forecasting for tropical cyclones threatening the United States, 1970–2001. *Bull. Amer. Meteor. Soc.*, **84**, 1197–1203.
- Goldenberg, S. B., and L. J. Shapiro, 1996: Physical mechanisms for the association of El Niño and West African rainfall with Atlantic major hurricane activity. *J. Climate*, **9**, 1169–1187.
- Gray, W. M., 1968: A global view of the origin of tropical disturbances and storms. *Mon. Wea. Rev.*, **96**, 669–700.
- , 1979: Tropical cyclone intensity determination through upper-tropospheric aircraft reconnaissance. *Bull. Amer. Meteor. Soc.*, **60**, 1069–1074.
- Hall, J. D., A. J. Matthews, and D. J. Karoly, 2001: The modulation of tropical cyclone activity in the Australian region by the Madden–Julian oscillation. *Mon. Wea. Rev.*, **129**, 2970–2982.
- Harr, P. A., and R. L. Elsberry, 1995: Large-scale circulation variability over the tropical western North Pacific. Part I: Spatial patterns and tropical cyclone characteristics. *Mon. Wea. Rev.*, **123**, 1225–1246.
- Hendon, H. H., and M. L. Salby, 1994: The life cycle of the Madden–Julian oscillation. *J. Atmos. Sci.*, **51**, 2225–2237.
- , B. Liebmann, M. Newman, J. D. Glick, and J. E. Schemm, 2000: Medium-range forecast errors associated with active episodes of the Madden–Julian oscillation. *Mon. Wea. Rev.*, **128**, 69–86.
- , M. C. Wheeler, and C. Zhang, 2007: Seasonal dependence of the MJO–ENSO relationship. *J. Climate*, **20**, 531–543.
- Herbert, P. J., and K. O. Potat, 1975: A satellite classification technique for subtropical cyclones. NOAA Tech. Memo., NWS SR-83, 25 pp.
- Higgins, R. W., and W. Shi, 2001: Intercomparison of the principal modes of interannual and intraseasonal variability of the North American monsoon system. *J. Climate*, **14**, 403–417.
- Inness, P., and J. M. Slingo, 2003: Simulation of the MJO in a coupled GCM. I: Comparison with observations and an atmosphere-only GCM. *J. Climate*, **16**, 345–364.
- Jarvinen, B. R., C. J. Neumann, and M. A. S. Davis, 1984: A tropical cyclone data tape for the north Atlantic basin, 1886–1983: Contents, limitations, and uses. NOAA Tech. Memo., NWS NHC-22, 28 pp.
- Jones, C., L. M. V. Carvalho, R. W. Higgins, D. E. Waliser, and J. K. E. Schemm, 2004: A statistical forecast model of tropical intraseasonal convective anomalies. *J. Climate*, **17**, 2078–2095.
- Jury, M. R., B. Pathack, and B. Parker, 1999: Climatic determinants and statistical prediction of tropical cyclone days in the southwest Indian Ocean. *J. Climate*, **12**, 1738–1746.
- Kalnay, E., and Coauthors, 1996: The NCEP/NCAR 40-Year Re-Analysis Project. *Bull. Amer. Meteor. Soc.*, **77**, 437–471.
- Kiladis, G. N., K. H. Straub, and P. T. Haertel, 2005: Zonal and vertical structure of the Madden–Julian oscillation. *J. Atmos. Sci.*, **62**, 2790–2809.
- Kim, J. H., C. H. Ho, H. S. Kim, C. H. Sui, and S. K. Park, 2008: Systematic variation of summertime tropical cyclone activity in the western North Pacific in relation to the Madden–Julian oscillation. *J. Climate*, **21**, 1171–1191.
- Klotzbach, P. J., 2007: Recent developments in statistical prediction of seasonal Atlantic basin tropical cyclone activity. *Tellus*, **59A**, 511–518.
- Knutson, T. R., and K. M. Weickmann, 1987: 30–60 day atmospheric oscillations: Composite life cycles of convection and circulation anomalies. *Mon. Wea. Rev.*, **115**, 1407–1436.
- Kossin, J. P., K. R. Knapp, D. J. Vimont, R. J. Murnane, and B. A. Harper, 2007: A globally consistent reanalysis of hurricane variability and trends. *Geophys. Res. Lett.*, **34**, L04815, doi:10.1029/2006GL028836.
- Kutzbach, J. E., 1967: Empirical eigenvectors of sea-level pressure, surface temperature and precipitation complexes over North America. *J. Appl. Meteor.*, **6**, 791–802.
- Landsea, C., 2007: Counting Atlantic tropical cyclones back to 1900. *Eos, Trans. Amer. Geophys. Union*, **88**, 197–202.
- Leroy, A., and M. C. Wheeler, 2008: Statistical prediction of weekly tropical cyclone activity in the Southern Hemisphere. *Mon. Wea. Rev.*, **136**, 3637–3654.
- Leslie, L. M., K. Fraedrich, and T. Glowacki, 1989: Forecasting the skill of a regional numerical weather prediction model. *Mon. Wea. Rev.*, **117**, 550–557.
- Liebmann, B., H. H. Hendon, and J. D. Glick, 1994: The relationship between tropical cyclones of the western Pacific and Indian Oceans and the Madden–Julian Oscillation. *J. Meteor. Soc. Japan*, **72**, 401–411.
- Lo, F., and H. H. Hendon, 2000: Empirical extended-range prediction of the Madden–Julian oscillation. *Mon. Wea. Rev.*, **128**, 2528–2543.
- Madden, R. A., and P. R. Julian, 1971: Detection of a 40–50-day oscillation in the zonal wind in the tropical Pacific. *J. Atmos. Sci.*, **28**, 702–708.
- , and —, 1972: Description of global-scale circulation cells in the tropics with a 40–50 day period. *J. Atmos. Sci.*, **29**, 1109–1123.
- , and —, 1994: Observations of the 40–50-day tropical oscillation—A review. *Mon. Wea. Rev.*, **122**, 814–837.
- Maloney, E. D., and D. L. Hartmann, 2000a: Modulation of eastern North Pacific hurricanes by the Madden–Julian oscillation. *J. Climate*, **13**, 1451–1460.
- , and —, 2000b: Modulation of hurricane activity in the Gulf of Mexico by the Madden–Julian Oscillation. *Science*, **287**, 2002–2004.
- Mancuso, R. L., 1967: A numerical procedure for computing fields of stream function and velocity potential. *J. Appl. Meteor.*, **6**, 994–1001.
- Mann, M. E., and K. A. Emanuel, 2006: Atlantic hurricane trends linked to climate change. *Eos, Trans. Amer. Geophys. Union*, **87**, 233–241.

- Matthews, A. J., 2000: Propagation mechanisms for the Madden-Julian Oscillation. *Quart. J. Roy. Meteor. Soc.*, **126**, 2637–2651.
- McBride, J. L., 1981: Observational analysis of tropical cyclone formation. Part I: Basic description of data sets. *J. Atmos. Sci.*, **38**, 1117–1131.
- Milliff, R. F., and R. A. Madden, 1996: The existence and vertical structure of fast, eastward-moving disturbances in the equatorial troposphere. *J. Atmos. Sci.*, **53**, 586–597.
- Mo, K. C., 2000: Intraseasonal modulation of summer precipitation over North America. *Mon. Wea. Rev.*, **128**, 1490–1505.
- , 2001: Adaptive filtering and prediction of intraseasonal oscillations. *Mon. Wea. Rev.*, **129**, 802–817.
- Molinari, J., and D. Vollaro, 2000: Planetary- and synoptic-scale influences on eastern Pacific tropical cyclogenesis. *Mon. Wea. Rev.*, **128**, 3296–3307.
- , D. Knight, M. Dickinson, D. Vollaro, and S. Skubis, 1997: Potential vorticity, easterly waves, and tropical cyclogenesis. *Mon. Wea. Rev.*, **125**, 2699–2708.
- Nakazawa, T., 1986: Mean features of 30–60 day variations as inferred from 8-year OLR data. *J. Meteor. Soc. Japan*, **64**, 777–786.
- , 1988: Tropical super cloud clusters within intraseasonal variations over the western Pacific. *J. Meteor. Soc. Japan*, **66**, 823–839.
- Powell, M. D., and S. D. Aberson, 2001: Accuracy of United States tropical cyclone landfall forecasts in the Atlantic basin (1976–2000). *Bull. Amer. Meteor. Soc.*, **82**, 2749–2768.
- Quan, X. W., P. J. Webster, A. M. Moore, and H. R. Chang, 2004: Seasonality in SST-forced atmospheric short-term climate predictability. *J. Climate*, **17**, 3090–3108.
- Ramsay, H., L. M. Leslie, P. J. Lamb, M. B. Richman, and M. Leplastrier, 2008: Interannual variability of tropical cyclones in the Australian region: Role of large-scale environment. *J. Climate*, **21**, 1083–1103.
- Rasmusson, E. M., and K. Mo, 1993: Linkages between 200-mb tropical and extratropical circulation anomalies during the 1986–1989 ENSO cycle. *J. Climate*, **6**, 595–616.
- Reichler, T., and J. O. Roads, 2005: Long-range predictability in the tropics. Part II: 30–60-day variability. *J. Climate*, **18**, 634–650.
- Sheets, R. H., 1990: The National Hurricane Center: Past, present and future. *Wea. Forecasting*, **5**, 185–232.
- Torrence, C., and G. P. Compo, 1998: A practical guide to wavelet analysis. *Bull. Amer. Meteor. Soc.*, **79**, 61–78.
- Vitart, F., S. Woolnough, M. A. Balmaseda, and A. M. Tompkins, 2007: Monthly forecast of the Madden–Julian oscillation using a coupled GCM. *Mon. Wea. Rev.*, **135**, 2700–2715.
- von Storch, H., and A. Smallegange, 1991: The phase of the 30- to 60-day oscillation and the genesis of tropical cyclones in the western Pacific. Max-Planck-Institut für Meteorologie, Rep. 66, 22 pp.
- Weare, B. C., and J. S. Nasstrom, 1982: Examples of extended empirical orthogonal function analysis. *Mon. Wea. Rev.*, **110**, 481–485.
- Webster, P. J., G. J. Holland, J. A. Curry, and H.-R. Chang, 2005: Changes in tropical cyclone number, duration, and intensity in a warming environment. *Science*, **309**, 1844–1846.
- Wheeler, M., and K. M. Weickmann, 2001: Real-time monitoring and prediction of modes of coherent synoptic to intraseasonal tropical variability. *Mon. Wea. Rev.*, **129**, 2677–2694.
- , and H. H. Hendon, 2004: An all-season real-time multivariate MJO index: Development of an index for monitoring and prediction. *Mon. Wea. Rev.*, **132**, 1917–1932.
- Wu, L., F. He, Z. Liu, and C. Li, 2007: Atmospheric teleconnections of tropical Atlantic variability: Interhemispheric, tropical-extratropical, and cross-basin interactions. *J. Climate*, **20**, 856–870.
- Zhang, C., 2005: Madden-Julian oscillation. *Rev. Geophys.*, **43**, RG2003, doi:10.1029/2004RG000158.
- Zhou, S., and A. J. Miller, 2005: The interaction of the Madden–Julian oscillation and the Arctic Oscillation. *J. Climate*, **18**, 143–159.